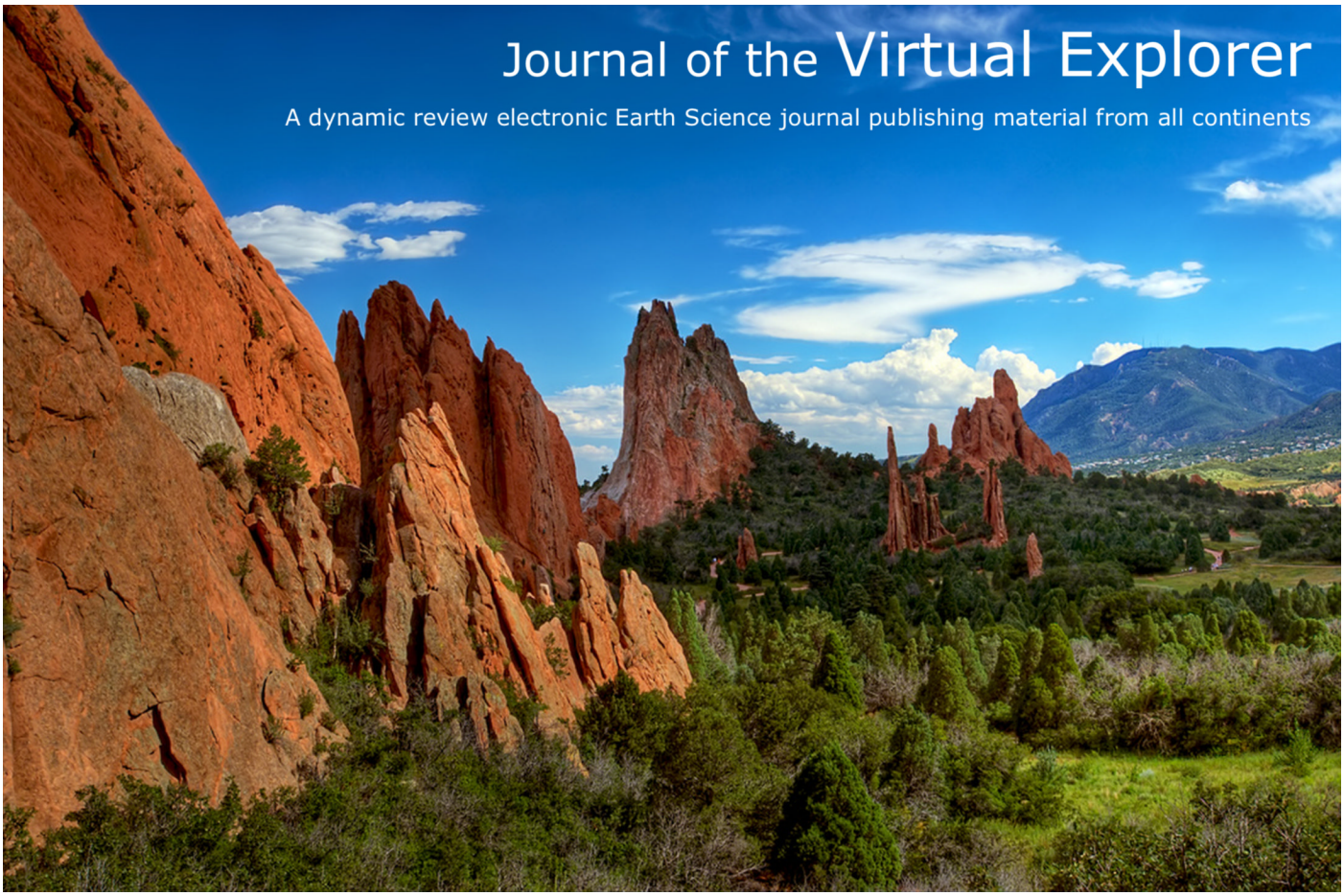

Dating fault fabrics using modern techniques of $^{40}Ar/^{39}Ar$ thermochronology: evidence for Paleozoic deformation in the Eastern Sierras Pampeanas, Argentina

Steven J. Whitmeyer

Journal of the Virtual Explorer, Electronic Edition, ISSN 1441-8142, volume **30**, paper 3
In: (Ed.) Declan De Paor, Making Sense of Shear (In honour of Carol Simpson), 2008.

Dating fault fabrics using modern techniques of $^{40}Ar/^{39}Ar$ thermochronology: evidence for Paleozoic deformation in the Eastern Sierras Pampeanas, Argentina

Steven J. Whitmeyer

Journal of the Virtual Explorer, Electronic Edition, ISSN 1441-8142, volume **30**, paper 3
In: (Ed.) Declan De Paor, Making Sense of Shear (In honour of Carol Simpson), 2008.

Abstract: New $^{40}Ar/^{39}Ar$ age data of ductile and brittle fault fabrics within the Sierras de Cordoba of the Eastern Sierras Pampeanas, Argentina, reveal episodes of Silurian and Early Carboniferous deformation. Laser ablation $^{40}Ar/^{39}Ar$ analyses of pseudotachylyte from the La Calera fault zone in the eastern Sierras de Córdoba yielded a weighted mean age of 429.3±3.5 Ma that is equivalent, within error, to existing age data. Pseudotachylyte from the Los Tuneles fault zone, along the northwestern margin of the Sierras de Córdoba, yielded weighted mean ages of 345±5 Ma and 348±2 Ma. These results are broadly coeval with ages of 341±5 Ma and 343±5 Ma obtained from ultramylonite biotite within the Tres Arboles fault zone along the southwestern margin of the Sierras de Córdoba.

These $^{40}Ar/^{39}Ar$ dates and kinematic data document Silurian brittle fault rocks that cross-cut regional metamorphic fabrics, and early Carboniferous ductile and brittle fault rocks that are interpreted as minimum ages for deformation. The close agreement between the ages for the Los Tuneles and Tres Arboles fabrics is consistent with existing models that equate the shallow, brittle fault fabrics of the Los Tuneles fault zone with deep, ductile fabrics of the Tres Arboles fault zone as a single extensive deformation zone along the western margin of the Sierras de Córdoba. The early Carboniferous deformation may represent the final stage of convergent tectonism along the western margin of Gondwana prior to the assembly of Pangaea.

http://virtualexplorer.com.au/article/2008/207/pampeanas-deformation

Citation: Whitmeyer, S. 2008. Dating fault fabrics using modern techniques of $^{40}Ar/^{39}Ar$ thermochronology: evidence for Paleozoic deformation in the Eastern Sierras Pampeanas, Argentina. In: (Ed.) Declan De Paor, *Journal of the Virtual Explorer*, volume **30**, paper 3, doi: 10.3809/jvirtex.2008.00207

Introduction

Micro-crystalline pseudotachylyte glass and fine-grained ultramylonite are frequent products of fault deformation (Sibson, 1977; Magloughlin and Spray, 1992), and precision geochronology of such materials can greatly assist in temporally constraining tectonic events. $^{40}Ar/^{39}Ar$ thermochronology of K-bearing fault materials has become an accepted method for dating deformation. However, standard $^{40}Ar/^{39}Ar$ analytical techniques are not well suited for dating pseudotachylyte or ultramylonite due to nuclear recoil effects and the likely incorporation of unwanted materials within analyses. Previous studies have shown that the nuclear recoil effect on fine-grained and/or altered biotite can yield $^{40}Ar/^{39}Ar$ ages older than the actual crystallization age of the mineral (Mitchell and Taka, 1984; Lo and Onstott, 1989; Ruffet et al., 1991). This is particularly problematic if the analyses are performed using conventional step-heating techniques, which can produce disturbed apparent age spectra (Ruffet et al., 1991; Roberts et al., 2001). Step-heating techniques also increase the potential for incorporating of undesirable materials in $^{40}Ar/^{39}Ar$ analyses of fine-grained fault rocks. Pseudotachylyte veins almost always include clasts of host rock material within the glassy matrix (Magloughlin and Spray, 1992), and analytical accuracy depends on avoiding as many of these clasts as possible. A similar problem is encountered when analyzing ultramylonite matrix materials, where the intended target mineral (such as biotite) is frequently less than 50μm in size, and intergrown with other minerals that are unsuitable for $^{40}Ar/^{39}Ar$ analyses.

The interpretation of age results from $^{40}Ar/^{39}Ar$ analyses of pseudotachylyte can be problematic as well. Several studies (e.g. Reimold et al., 1990; Kelley et al., 1994; Thompson et al., 1998) have interpreted at least some $^{40}Ar/^{39}Ar$ ages obtained from pseudotachylyte samples as crystallization ages that directly provide the time of fault movement. However, recent work suggests that pseudotachylyte glass may have a closure temperature of 175˚C or less for argon gas retention (Hazelton et al., 2003). Since $^{40}Ar/^{39}Ar$ ages from mid-crustal fault rocks may record the time of regional cooling below 175˚C rather than the actual period of fault movement, an estimation of the ambient temperature of host rocks during faulting is critical for the correct interpretation of $^{40}Ar/^{39}Ar$ ages.

This study uses excimer (uv) laser-probe spot fusion $^{40}Ar/^{39}Ar$ thermochronology to analyze pseudotachylyte and very fine-grained ultramylonite biotite. Pseudotachylyte and ultramylonite were sampled from the La Calera, Los Tuneles and Tres Arboles fault zones located in the Sierras de Córdoba, central Argentina (Figure 1). The La Calera results are compared with existing $^{40}Ar/^{39}Ar$ ages from the same fault zone (Northrup et al., 1998) to evaluate whether comparable results can be obtained using excimer laser probe fusion techniques. Existing $^{40}Ar/^{39}Ar$ thermochronology in the region of the Los Tuneles and Tres Arboles fault zones provides a framework within which these $^{40}Ar/^{39}Ar$ results are evaluated to determine whether they represent geologically reasonable ages for fault movement, or, conversely, represent regional cooling of pseudotachylyte and/or fine-grained biotite below their closure temperatures. Age results from the Los Tuneles pseudotachylytes are compared with biotite ages from the Tres Arboles ultramylonites to evaluate an existing model that depicts the Los Tuneles and Tres Arboles fault zones as a continuous, north-striking deformation zone, which is exposed through a range of crustal depths from 10-12km in the north to 18-22 km in the south (Whitmeyer and Simpson, 2003). Finally, the implications of these age results are evaluated in the context of early to middle Paleozoic tectonism along the western margin of Gondwana.

Geologic Setting

The Tres Arboles and Los Tuneles fault zones collectively extend for more than 250km along the western margin of the Sierras de Córdoba (Simpson et al., 2003; Whitmeyer and Simpson, 2003; Figure 1). These faults likely facilitated the Paleozoic juxtaposition of the two principal components of the Eastern Sierras Pampeanas: The Sierras de Córdoba terrane in the east and the Sierra de San Luis terrane in the west (Whitmeyer and Simpson, 2003; 2004). The Early-Middle Paleozoic was a period of protracted convergence along the western margin of Gondwana (Ramos, 1988), and the assembly of the Eastern Sierras Pampeanas is likely coeval with one or more significant tectonic events that affected Gondwana, such as the Famatinian (Aceñolaza and Toselli, 1988), and Achalian (Sims et al., 1998) orogenies.

Figure 1. Simplified geologic map

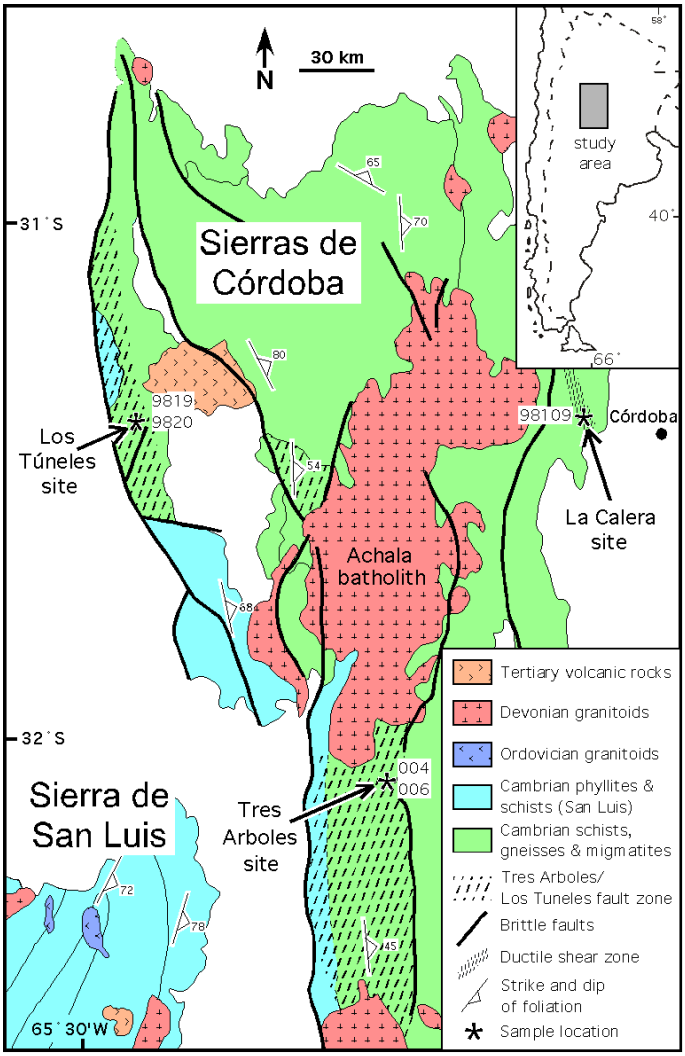

Simplified geologic map of the Sierras de Córdoba and northeastern portion of the Sierra de San Luis, Argentina. Los Tuneles, La Calera and Tres Arboles sample locations indicated by arrows.

Cenozoic uplift and exhumation of the Sierras de Córdoba have exposed crustal depths of 10-12km along the Los Tuneles fault zone in the northwest (Simpson et al., 2003), and 18-22km along the Tres Arboles fault zone in the southwest (Whitmeyer and Simpson, 2003). The Los Tuneles fault zone thrusts biotite+garnet+sillimanite schists to the west over biotite+chlorite phyllites (Simpson et al., 2003). Greenschist-facies S/C mylonites predominate within a several-hundred-meter-thick shear zone and are overprinted by cataclastic fabrics directly above the thrust contact. Within this region cm-thick pseudotachylyte veins intrude both parallel and at a high angle to mylonitic fabrics and host-rock foliation (Figure 2a). The Tres Arboles fault zone consists of a 16km-thick zone of mylonites and abundant ultramylonites that juxtapose high-grade gneisses and migmatites of the southern Sierras de Córdoba against biotite quartzites of San Luis affinity (Whitmeyer and Simpson, 2003; Figure 1).

Figure 2. Los Tuneles fault zone

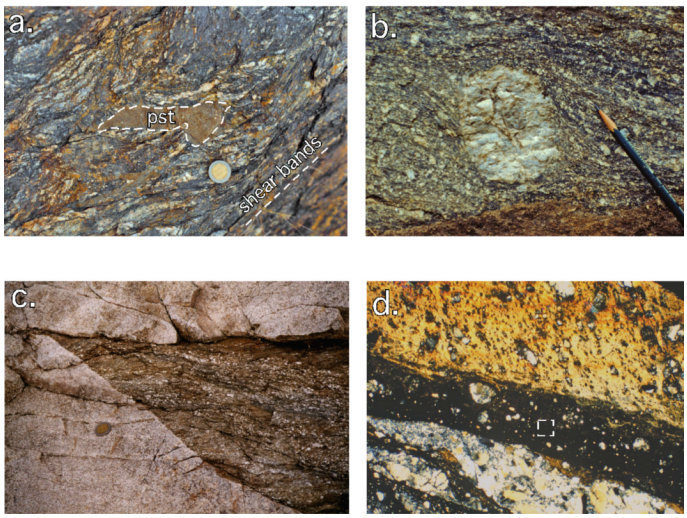

(a) Outcrop photo of Los Tuneles fault zone, showing pseudotachylyte vein cross-cutting greenschist-facies S/C mylonite. (b) Outcrop photo of sigma feldspar grain in Tres Arboles fault zone mylonites. (c) Outcrop photo of Achala-related granite truncating Tres Arboles fault zone ultramylonites. (d) Photomicrograph of dark brown pseudotachylyte vein (analyzed) intruding light brown pseudotachylyte + cataclasite, La Calera fault zone; representative 300 µm raster square indicated in pseudotachylyte vein. Plane light. Coin for scale in (a), (c) = 2.5 cm; pencil length in (b) = 4 cm.

The La Calera fault zone extends for several kilometers along the northeastern margin of the Sierras de Córdoba (Figure 1), and includes several discrete, meters-thick zones of amphibolite-facies mylonitic and ultramylonitic rocks (Simpson et al., 2003). Greenschist-facies S/C fabrics overprint higher-grade ultramylonites and contain local, cm-thick pseudotachylyte veins that are mostly subparallel to the mylonitic fabric (Figure 2b). Northrup et al. (1998) reported a $^{40}Ar/^{39}Ar$ age of 428±12 Ma from pseudotachylyte in this zone.

Sample Characteristics

The La Calera pseudotachylyte sample (98109) was chosen to test whether existing $^{40}Ar/^{39}Ar$ ages of pseudotachylyte from this fault zone could be replicated using excimer laser-probe techniques. Two generations of pseudotachylyte are evident within the La Calera zone: a

centimeters-thick, light brown pseudotachylyte with abundant quartz and feldspar-dominated lithic fragments (upper half of Figure 2b), and a dark brown, millimeters-thick pseudotachylyte that intrudes and crosscuts the thicker, light brown pseudotachylyte veins (center to lower right of (Figure 2b). The darker pseudotachylyte is visibly more homogenous with apparently fewer clasts and fragments and therefore was chosen for analysis. Lithic fragments within the darker pseudotachylyte include quartz±feldspar clasts and fragments of the light brown pseudotachylyte.

Pseudotachylyte samples from the Los Tuneles fault zone (9819, 9820) consist of dark, cryptocrystalline matrix with abundant cataclastic fragments of host rock. Clasts are predominantly quartz±feldspar, range from sub-microscopic to 500µm in diameter, and are uniformly distributed in center regions of pseudotachylyte veins (Figure 2c). Vein margins are composed of a much higher proportion of host-rock fragments (lower half of Figure 2c) and consequently were avoided in these analyses.

Ultramylonite samples (004, 006) contain a very fine-grained (~5-30µm) matrix of biotite±plagioclase±quartz, with 100-200µm, rounded porphyroblasts of plagioclase ±garnet (Figure 2d). Close examination of the matrix fabric reveals mostly random, interlocking grains with little evidence of a well-defined foliation. $^{40}Ar/^{39}Ar$ analyses were performed on 10-20µm matrix biotite and avoided relict, coarser-grained biotite that occurs adjacent to, or as inclusions within, garnet porphyroblasts.

$^{40}Ar/^{39}Ar$ Results

Pseudotachylyte samples were probed with a 42µm beam and rastered over a 300µm-square region that minimized the incorporation of cataclastic fragments (Figure 2c). A total of 13 individual analyses from the La Calera pseudotachylyte sample (98109) produced a weighted mean age of 429.3±3.5 Ma ((Table 1); Figure 3). This result is coincident, within error, with an inverse isochron age of 428±12 Ma reported by Northrup et al. (1998). Analyses of 16-18 spots from the Los Tuneles pseudotachylyte samples (9819, 9820) yielded weighted mean ages of 345.0±5.1 Ma and 348.2±2.2 Ma, respectively (Table 1; Figure 3).

Table 1. Cumulative weighted mean age results for pseudotachylyte and ultramylonite samples, including sampling locations and number of individual spots analyzed for each sample by laser spot fusion. Errors reported at 2 sigma. See Fig. 1 for sampling locations.

Sample	Material	Location	No. of spots analyzed	Age (Ma) ± 2σ
004	ultramylonite biotite	Tres Arboles	15	340.6 ± 5.4
006	ultramylonite biotite	Tres Arboles	19	342.5 ± 5.3
9819	pseudotachylyte	Los Tuneles	16	345.0 ± 5.1
9820	pseudotachylyte	Los Tuneles	18	348.2 ± 2.2
98109	pseudotachylyte	La Calera	13	429.3 ± 3.5

Figure 3. Sample 9819

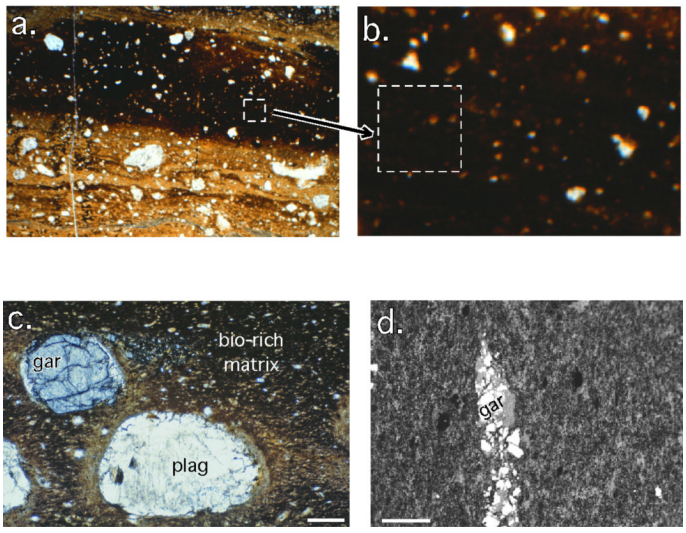

(a) Photomicrograph of pseudotachylyte sample 9819, with representative 300 µm raster square indicated. Plane light. (b) Enlargement of sampling region of (a), illustrating cataclastic fragments inadvertently incorporated within 300 µm raster square. Plane light. (c) Photomicrograph of ultramylonite sample 004, with representative biotite-rich matrix indicated. Plane light. (d) Backscatter electron image of ultramylonite sample 004, showing relict garnet fragments (white) within a biotite + plagioclase ± quartz matrix. Note that in this image light gray = biotite, medium gray = plagioclase, dark gray = quartz. Scale bars for (c) = 50 µm; (d) = 100 µm.

Tres Arboles ultramylonite samples were probed with a 30μm beam along 3-4 discrete lines that followed regions of biotite-rich matrix (Figure 2d). 15-19 individual analyses of fine-grained biotite from ultramylonite samples 004 and 006 yielded weighted mean ages of 340.6±5.4 Ma and 342.5±5.3 Ma, respectively (Table 1, Figure 3)). Analytical procedures and data from individual analyses are detailed in Appendix A.

Discussion

The primary difficulty in $^{40}Ar/^{39}Ar$ analyses of very fine-grained materials, such as pseudotachylyte and ultramylonitic biotite, is the high probability of incorporating undesirable minerals or cataclastic fragments. Laser beam diameters of 30-42μm enabled the ablation of a spot less than 50μm in width, which was either rastered over a square region or tracked along predefined lines. This flexibility and ability to predetermine the path of the laser made avoiding optically-visible foreign materials fairly straightforward. The advantages of this technique are apparent in the close precision among individual analyses of a given sample, and this precision is reflected in small 2σ error constraints on weighted mean ages (Table 1). However, the size distribution of cataclastic fragments within pseudotachylyte veins can include submicroscopic fragments (Figure 2c). Many of the analyzed raster squares likely contained a few submicroscopic clasts, which produced significant errors in some of the individual analyses (e.g. analyses 6, 7, 15 of sample 9819, Table AP2).

The fine-grained matrix of the ultramylonite samples is composed primarily of biotite but also contains plagioclase and occasional quartz grains (Figure 2d). Although the laser beam was tracked through predominantly biotite regions, the heterogeneous, interlocking fabric of the matrix meant that incorporation of some plagioclase±quartz was unavoidable. Other complications included occasional mistracking of the laser when it reached a turning node in the predetermined path, which sometimes resulted in the partial ablation of undesirable minerals. This is reflected in large errors on some of the individual ultramylonite analyses (e.g. analyses 1, 6, 7 of sample 006, Table AP1)).

The use of a small diameter laser beam for spot fusion makes it difficult to generate Ar gas in sufficient volumes to achieve a high signal-to-noise ratio (Roberts et al., 2001). The very fine-grained target materials in these samples necessitated the use of 30-42μm beams, which required high current intensities (28-30kV) for long durations (8-12 minutes) to enable the accumulation of sufficient Ar gas for robust analyses. Analyses that fell below a threshold of 70% 40Ar lacked sufficient gas for robust results and therefore were discarded (see asterisk-marked analyses, (Table AP1 and Table AP2). Low gas yields on several of the individual analyses above the 70% threshold still produced significant errors greater than ±30 Ma (e.g. analyses 004: 1; 006: 1, 6, 7; and 9819: 6, 7, 12, 15; Table AP1 and Table AP2). These low yields likely resulted from a poor choice of analysis area and/or occasional mistracking of the laser, which allowed undesirable clasts or minerals to be partially ablated.

Nuclear recoil during sample irradiation can result in the transfer of ^{39}Ar from K-rich minerals to adjacent K-poor minerals (Turner and Cadogan, 1974, Onstott et al., 1995), which would artificially increase the apparent ages of analyzed K-rich minerals. Recoil distances have been estimated at approximately 0.08μm across a mineral boundary (Villa, 1997), and thus can be a factor for concern when dating fine-grained minerals such as the 10-20μm biotite in the ultramylonite samples. The possible recoil influence was minimized in these analyses by using an excimer (uv) laser to target the centers of biotite-rich areas, and avoid marginal regions which are more susceptible to ^{39}Ar loss (e.g. Roberts et al., 2001). In the ultramylonite samples the matrix is predominately biotite, so most ^{39}Ar transfer due to recoil would simply exchange ^{39}Ar between adjacent biotite grains, and therefore result in little net loss. A small percentage of K-poor minerals, such as plagioclase±quartz, occur within the ultramylonitic matrix and may have absorbed a fraction of the recoil-produced ^{39}Ar, thus yielding artificially older apparent ages. However, the generally good agreement among individual analyses within each sample suggests that nuclear recoil was not a significant factor in the weighted mean age results.

Interpretation of $^{40}Ar/^{39}Ar$ age results

The Silurian age (429.3±3.5 Ma) obtained from the La Calera pseudotachylyte sample (98109) is coincident, within error, with the published age of this fault zone (428±12 Ma; Northrup et al., 1998), and calculated ages from all of the individual analyses in this sample lie within the error range of the Northrup et al. (1998) results. This concordance suggests that the excimer laser

technique for dating pseudotachylyte is capable of producing results in line with other established techniques. In addition, the lower error constraints on the cumulative age produced by excimer probe analyses highlight the potential advantages of this technique for fine-grained materials.

Figure 4. Frequency distribution plot

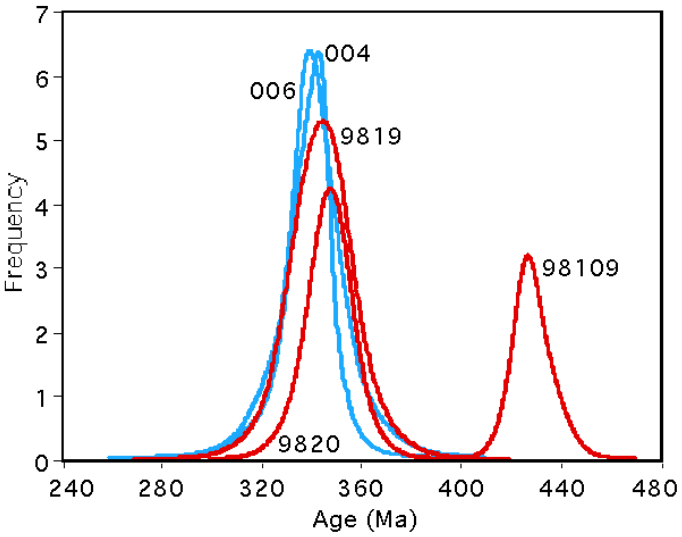

Frequency distribution plot of $^{40}Ar/^{39}Ar$ age results from all pseudotachylyte and ultramylonite samples. Peaks indicate 2σ error range for individual spot analyses of each sample.

The closure temperature for Ar-retention in pseudotachylyte is not nearly as well-defined as for K-bearing minerals such as amphibole and muscovite (McDougall and Harrison, 1999; c.f. Carroll, 1991). Recent experimental analyses by Hazelton et al. (2003) suggest that the closure temperature for high-silica, low-CaFeMg pseudotachylyte glass is no higher than 175˚C. An estimation of the ambient temperature of pseudotachylyte host rocks can be obtained with the geothermometer of O'Hara (2001). Temperatures of 250-253˚C (Table AP3) were calculated for the Los Tuneles samples, which is greater than the Hazelton et al. (2003) closure temperature for pseudotachylyte. The predominantly quartzofeldspathic composition of the Los Tuneles host-gneisses likely falls within the high-silica category of Hazelton et al. (2003), and therefore the Los Tuneles results may represent regional cooling ages that are younger than the actual period of fault movement.

Existing $^{40}Ar/^{39}Ar$ thermochronology indicates that regional ambient temperatures along the Tres Arboles fault zone dropped below the amphibole closure temperature (~500˚C; McDougall and Harrison, 1999) no later than 478 Ma, through the standard closure temperature for biotite (~300-350˚C) by 440 Ma, and below 250˚C by about 380 Ma (Northrup et al, 1998; Krol and Simpson, 1999). These constraints indicate that host rocks were cooler at the time of faulting than the standard closure temperature for medium-grained biotite. However, recalibration of the closure temperature for 10-20μm biotite grains, using the equation from Dodson (1973), yielded temperatures of 237-252˚C (Table AP4), similar to host-rock temperatures. Therefore, it is possible that the $^{40}Ar/^{39}Ar$ biotite ages represent regional cooling below about 250˚C, instead of directly dating movement along the fault zone.

Existing $^{40}Ar/^{39}Ar$ thermochronology (Northrup et al, 1998; Krol and Simpson, 1999) suggests that regional cooling of the western margin of the Sierra de Córdoba progressed at an approximate rate of 4 - 5˚C/m.y. during the Late Cambrian to Middle Ordovician. If these cooling rates were consistent throughout the Middle Paleozoic, the $^{40}Ar/^{39}Ar$ ages presented here would underestimate the period of fault zone movement by a maximum of 20 million years. Thus, deformation in the Los Tuneles and Tres Arboles fault zones may have occurred as early as 368 Ma and 363 Ma, respectively. This is consistent with existing K-Ar ages for amphiboles from the Los Tuneles fault zone that yielded ages of 373 ± 11 Ma and 365 ± 10 Ma (Rapela et al., 1998).

$^{40}Ar/^{39}Ar$ ages from the Los Tuneles pseudotachylyte samples (348-345 Ma) are 3-8 million years older than those obtained from the Tres Arboles ultramylonites (343-341 Ma), although error constraints allow for overlap between almost all of the samples. The small age discrepancy may represent slight differences in the time of movement between the fault zones, or it may be due to differences in the cooling temperature profiles of pseudotachylyte versus fine-grained biotite. Either way, the coincidence, within error, of $^{40}Ar/^{39}Ar$ ages from the northern Los Tuneles fault zone and the southern Tres Arboles fault zone is consistent with the existing model, which depicts one extensive deformation zone along most of the western margin of the Sierras de Córdoba (Whitmeyer and Simpson, 2003).

Intrusive rocks of the Achala batholith suite truncate deformation fabrics of the Tres Arboles fault zone (Figure 2c), which implies that movement along the zone must have ceased prior to 368 ± 2 Ma (Dorais et al.,

1997). The U/Pb zircon crystallization age for the Achala batholith was obtained from samples in the central "Achala series" (Demange et al., 1993) section of the poly-phase granitoid. However, field relations suggest that undated southwestern regions of the batholith (the "Cumbrecita" and "Champaquí series") that cross-cut the Tres Arboles fault zone (Figure 2c) are the youngest of the Achala-related intrusions, and may postdate the Late Devonian - Early Carboniferous estimates of movement along the fault zone reported here.

The constraints on the regional ambient temperature at the time of pseudotachylyte and ultramylonite generation suggest that the early Carboniferous age results may reflect regional cooling and not directly date the time of deformation. Thus, these results are interpreted as minimum ages for movement along the Los Tuneles and Tres Arboles fault zones. Regional cooling rate estimates allow for reactivation as early as 368 Ma, which would temporally equate late movement along the fault zones with intrusion of the Achala batholith. An important consideration is that $^{40}Ar/^{39}Ar$ analyses in both the Los Tuneles and Tres Arboles fault zones date reactivation fabrics and provide no temporal constraints on earlier phases of deformation in either zone.

Tectonic Implications

Middle - Late Devonian plutonism has been documented across the Eastern Sierras Pampeanas, with potentially correlative deformation restricted to local reactivation of existing fault zones (Dorais et al., 1997; Sims et al., 1998; Whitmeyer and Simpson, 2003). Mylonitic and ultramylonitic fabrics along the Tres Arboles fault zone and pseudotachylyte veins along the Los Tuneles fault zone strongly overprint earlier ductile deformation fabrics (Simpson et al., 2003). This suggests that the Late Devonian - Early Carboniferous ages reported here represent more extensive movement during fault zone reactivation than was previously thought. $^{40}Ar/^{39}Ar$ thermochronology of fault zone reactivation fabrics from this study suggest that ultramylonites of the Tres Arboles fault zone are likely correlative with brittle fault zone fabrics in the Los Tuneles zone but provide no constraints on earlier deformation in either area. These age results constrain the final juxtaposition of the Sierra de San Luis southwest of the Sierras de Córdoba to no later than Early Carboniferous, possibly as part of the Achalian orogeny of Sims et al. (1998) and possibly the accretion of the Chilenia terrane farther west (Davis et al., 1999). This event likely represents the last phase of the early to middle Paleozoic collisional sequence along the western margin of Gondwana, prior to the final assembly of Pangaea in the late Paleozoic.

Acknowledgements

Thanks to Carol Simpson for exposure to the field areasand discussions on tectonic implications, and Kip Hodges and Xifan Zhang for advice and guidance on analytical techniques. This research was partially funded by NSF grant EAR 9628158 to C. Simpson and L. P. Gromet.

Appendix A

Analytical Procedures

$^{40}Ar/^{39}Ar$ laser fusion analyses were conducted at the Clair argon laboratory, MIT using procedures similar to those described in Hodges and Bowring (1995). 100μm-thick, polished sample sections were cut into 0.5cm-square pieces and packaged in aluminum foil for irradiation. Samples were irradiated in the C5 position of the McMaster University nuclear reactor for 10 hours with a total power of 20MW. The conversion efficiency of 39K to ^{39}Ar was monitored using Taylor Creek rhyolite with an assumed age of 28.34 Ma (Renne et al., 1998). K_2SO_4 and CaF_2 synthetic salts were used to enable corrections for interfering nuclear reactions. Samples were fused with a New Wave Research/Mechantek Nd-YAG (ArF) excimer (uv) laser at a current intensity of 28-30kV for 8-12 minutes. Each pseudotachylyte sample site was probed with a 42μm beam, rastered over a 300μm-square area that was chosen to minimize the incorporation of cataclastic fragments. Ultramylonite samples were probed with a 30μm beam along 3-4 discrete lines per analysis. Each line was chosen to track regions of biotite-rich matrix and avoid very fine-grained (~5-15μm) plagioclase and occasional quartz. Released gasses were purified for 10-15 minutes with Al-Zr and Fe-Zr-V getters and then admitted into a MAP 215-50 mass spectrometer for Ar isotopic analysis using an electron multiplier. System blanks were measured before and after each sample, and all data were corrected for blanks and mass-fractionation effects. Final data reduction was conducted with the program ArArCalc (Koppers, 2002). The integrated $^{40}Ar/^{39}Ar$ age for each sample was calculated as a (% ^{39}Ar) weighted mean of 13-19 individual analyses, and

sample errors were calculated as standard errors of the weighted mean. Precision limits represent propagated measurement uncertainties and are reported at the ee level.

AP1

$^{40}Ar/^{39}Ar$ analytical data for fine-grained biotite from ultramylonite samples. $^{40}Ar^*$ is radiogenic ^{40}Ar. Weighted age is the mean age of individual analyses weighted on ^{39}Ar (%). Individual analyses numbers preceded by a '*' were not used when calculating the weighted age.

Table AP1.

ID	$^{39}Ar/^{40}Ar$	$^{36}Ar/^{40}Ar$	$^{40}Ar^*$ (%)	^{39}Ar (%)	Age (Ma ± 2σ)
	004 Tres Arboles ultramylonite, J=0.0151				
1	0.0739	0.000453	88.20	2.81	335.60 ± 46.06
2	0.0748	0.000740	82.06	5.33	331.67 ± 29.54
3	0.0734	0.000365	90.26	4.90	337.58 ± 12.60
4	0.0735	0.000349	90.65	7.03	337.17 ± 12.50
5	0.0715	0.000385	89.79	9.79	345.83 ± 15.28
6	0.0720	0.000417	89.03	8.70	343.31 ± 6.16
7	0.0724	0.000746	81.93	6.24	341.96 ± 11.22
8	0.0722	0.000273	92.53	6.55	342.76 ± 12.98
9	0.0728	0.000411	89.16	6.12	339.90 ± 13.18
10	0.0737	0.000489	87.37	6.65	336.23 ± 11.04
11	0.0741	0.000506	86.98	5.06	334.42 ± 17.46
12	0.0762	0.000737	82.11	2.56	326.34 ± 29.50
13	0.0719	0.001123	75.08	3.19	344.09 ± 22.66
14	0.0715	0.000205	94.28	13.40	345.71 ± 5.16
15	0.0722	0.000578	85.41	11.66	342.72 ± 16.30
*16	0.0921	0.001480	69.70	2.56	273.97 ± 41.54
*17	0.1023	0.001860	64.63	3.77	248.48 ± 56.12
*18	0.0992	0.001781	65.49	5.98	255.52 ± 29.76
	weighted age	**(n=15)**			**340.60 ± 5.40**
ID	**$^{39}Ar/^{40}Ar$**	**$^{36}Ar/^{40}Ar$**	**$^{40}Ar^*$ (%)**	**^{39}Ar (%)**	**Age (Ma ± 2σ)**

AP2

$^{40}Ar/^{39}Ar$ analytical data for pseudotachylyte samples. $^{40}Ar^*$ is radiogenic ^{40}Ar. Weighted age is the mean age of individual analyses weighted on ^{39}Ar (%). Individual analyses numbers preceded by a '*' were not used when calculating the weighted age.

Table AP2.

ID	$^{39}Ar/^{40}Ar$	$^{36}Ar/^{40}Ar$	$^{40}Ar^*$ (%)	^{39}Ar (%)	Age (Ma ± 2σ)
	9819 Los Tuneles pseudotachylyte, J=0.0153				
1	0.0714	0.000480	87.57	4.09	350.31± 23.64
2	0.0710	0.000563	85.74	6.89	352.17 ± 11.38
3	0.0704	0.000625	84.40	6.06	354.70 ± 22.02
4	0.0742	0.000762	81.61	8.37	338.30 ± 15.86
5	0.0749	0.000814	80.61	9.41	335.43 ± 14.18
6	0.0746	0.001091	75.62	8.09	336.73± 35.66
7	0.0704	0.000495	87.24	5.24	354.75 ± 34.28
8	0.0720	0.000717	82.51	9.47	347.77 ± 19.34
9	0.0739	0.000380	89.90	2.76	339.38 ± 25.50
10	0.0723	0.000707	82.72	7.29	346.49 ± 13.92
11	0.0730	0.001160	74.47	5.63	343.44 ± 14.50
12	0.0724	0.000928	78.47	6.19	346.07 ± 34.16
13	0.0736	0.000906	78.87	3.47	340.56 ± 27.54
14	0.0721	0.001009	77.03	8.18	347.37 ± 25.36
15	0.0721	0.000875	79.45	4.81	347.11 ± 46.58
16	0.0730	0.000684	83.17	4.06	343.39 ± 18.84
ID	**weighted age $^{39}Ar/^{40}Ar$**	**(n=16) $^{36}Ar/^{40}Ar$**	**$^{40}Ar^*$ (%)**	**^{39}Ar (%)**	**344.95 ± 5.08 Age (Ma ± 2σ)**
	9820 Los Tuneles pseudotachylyte, J=0.0155				
1	0.0728	0.001043	76.44	2.09	348.02 ± 16.64

AP3

Calculated ambient host rock temperature for samples 9819 and 9820 at the time of pseudotachylyte generation. Method follows that of O'Hara (2001) and uses the volume ratio of clast fragments/matrix (W/M) to calculate the temperature (Tlow) with the equation: W/M = (Thigh – Tlow) / Thigh. Melting temperature (Thigh) ~ 927˚C, and 2 sigma errors for Tlow are estimated at ±70˚C (O'Hara, 2001).

Table AP3.

Sample	Number of points	Clast points	Matrix points	Clast/ matrix ratio	Calculated Temperature
9819	210	77	133	0.579	232 ± 70˚C
9820	203	73	130	0.562	253 ± 70˚C

AP4

Calculated Ar closure temperatures for 10μm and 20μm biotite grains using the equation of Dodson (1973):

$$T_c = \frac{\frac{E}{R}}{ln\left[\frac{(A \cdot R \cdot T_c^2 \cdot (\frac{D_0}{a^2}))}{E(\frac{dT}{dt})}\right]}$$

with analytical constants from Harrison et al. (1985). Convergence of calculated temperatures (Tc) was easily reached within 4 iterations.

Constants (Ann56 biotite values from Harrison et al., 1985):

E (activation energy) = 47 kcal/mol
D_0 (frequency factor) = 0.077
A (geometry = infinite cylinder) = 27
dT/dt (linear cooling rate) = 5˚C/m.y.

Table AP4.

Radius of grain (μm)	Number of iterations	Closure temperature
10	4	236.6˚C
20	4	251.6˚C

References

Aceñolaza, F. G., and A. J. Toselli, 1988, El sístema de Famatina, Argentina: su interpretación como orogeno de margen continental achvo, in 5 Congreso Geológico Chileno, 1, A55-A67, 115-138, Santiago.

Carroll, M. R., 1991, Diffusion of argon in rhyolite, orthoclase, and albite composition glasses: Earth and Planetary Science Letters, v. 103, p. 156-168.

Davis, J. S., Roeske, S. M., McClelland, W. C., Snee, L. W., 1999, Closing the ocean between the Precordillera terrane and Chillenia: Early Devonian ophiolite emplacement and deformation in the southwest Precordillera. Laurentia-Gondwana Connections before Pangea, Ramos V. A., Keppie, J. D. (Eds.). Geological Society America, Special Paper 336, p. 115-138.

Demange, M., Alvarez, J.O., Lopez, L., and Zarco, J., 1993, Existencia de series magmaticas diferentes en el batolito del Achala (Córdoba, Argentina): Tri Actas XII, Congreso Geologico Argentina II, Congreso Exploracion Hidrocarburos IV, p. 23-29.

Dodson, M.H., 1973, Closure temperature in cooling geochronological and petrological systems: Contributions to Mineralogy and Petrology, v. 40, p. 259-274.

Dorais, M.J., Lira, R., Chen, Y., and Tingey, D., 1997, Origin of biotite-apatite-rich enclaves, Achala Batholith, Argentina: Contributions to Mineralogy and Petrology, v. 130, p. 31-46.

Harrison, T.M., Duncan, I., and McDougall, I., 1985, Diffusion of ^{40}Ar in biotite: Temperature, pressure and compositional effects: Geochimica et Cosmochimica Acta, v. 49, p. 2461-2468.

Hazelton, G.B., Axen, G., and Lovera, O., 2003, Argon retention properties of silicate glasses and implications for ^{40}Ar/^{39}Ar age and noble gas diffusion studies: Contributions to Mineralogy and Petrology, v. 145, p. 1-14.

Hodges, K.V. and Bowring, S.A., 1995, ^{40}Ar/^{39}Ar thermochronology of isotopically zoned micas: Insight from the southwestern USA Proterozoic orogen: Geochimica et Cosmochimica Acta, v. 59, p. 3205 –3220.

Kelley, S.P., Reddy, S.M., and Maddock, R., 1994, Laser-probe ^{40}Ar/^{39}Ar investigation of a pseudotachylyte and its host rock from the Outer Isles Thrust, Scotland: Geology, v. 22, p. 443-446.

Koppers, A.A.P., 2002, ArArCalc-software for ^{40}Ar/^{39}Ar age calculation: Computer Geosciences, v. 28, p. 605-619.

Krol, M. A., and Simpson, C. , 1999, ^{40}Ar/^{39}Ar Cooling ages from micas in the eastern Sierras Pampeanas accretionary prism rocks: Geological Society of America Abstracts with Programs, v. 31, p. 114-115.

Lo, C.H., and Onstott, T.C., 1989, ^{39}Ar recoil artifacts in chloritized biotite: Geochimica et Cosmica Acta, v. 53, p. 2697-2711.

Magloughlin, J. F., and Spray, J. G., 1992, Frictional melting processes and products in geological materials: Introduction and discussion: Tectonophysics, v. 204, p. 197-204.

McDougall, I., and Harrison, T.M., 1999, Geochronology and thermochronology by the ^{40}Ar/^{39}Ar method: Oxford University Press, New York.

Mitchell, J.G., and Taka, A.S., 1984, Potassium and argon loss patterns in weathered micas: Implications for detrital mineral studies, with particular reference to the Triassic palaeogeography of the British Isles: Sedimentary Geology, v. 39, p. 27-52.

Northrup, C.J., Simpson, C., and Hodges, K.V., 1998, Pseudotachylyte in fault zones of the Sierras de Córdoba, Argentina: Petrogenesis and ^{40}Ar/^{39}Ar geochronology: Geological Society of America Abstracts with Programs, v. 30, p. 325.

O'Hara, K.D., 2001, A pseudotachylyte geothermometer: Journal of Structural Geology, v. 23, p. 1345-1357.

Onstott, T.C., Miller, M.L., Ewing, R.C., Arnold, G.W., and Walsh, D.S., 1995, Recoil refinements: implications for the ^{40}Ar/^{39}Ar dating technique: Geochimica et Cosmica Acta, v. 59, p. 1821-1834.

Ramos, V. A., 1988, Late Proterozoic-Early Paleozoic of South America - a collisional history: Episodes, v. 11, p. 168-174.

Rapela, C. W., Pankhurst, R. J., Casquet, C., Baldo, E., Saavedra, J., Galindo, C., Fanning, C. M., 1998, The Pampean Orogeny of the southern proto-Andes: Cambrian continental collision in the Sierras de Córdoba, in The Proto-Andean Margin of Gondwana, Pankhurst, R. J., Rapela, C. W. (Eds.). Geological Society of London, Special Publication 142, p. 181-218.

Reimold, W.U., Jessberger, E.K., and Stephan, T., 1990, ^{40}Ar/^{39}Ar dating of pseudotachylyte from the Vredefort Dome, South Africa; a progress report: Tectonophysics, v. 171, p. 139-152.

Renne, P.R., Swisher, C.C., Deino, A.L., Karner, D.B., Owens, T., and DePaolo, D.J., 1998, Intercalibration of standards, absolute ages and uncertainties in ^{40}Ar/^{39}Ar dating: Chemical Geology (Isotope Geosciences), v. 145, p. 117-152.

Roberts, H.J., Kelley, S.P., and Dahl, P.S., 2001, Obtaining geologically meaningful ^{40}Ar/^{39}Ar ages from altered biotite: Chemical Geology, v. 172, p. 277-290.

Ruffet, G., Féraud, G., and Amouric, M., 1991, Comparison of ^{40}Ar/^{39}Arconventional and laser dating of biotites from the North Trégor Batholith: Geochimica et Cosmica Acta, v. 55, p. 1675-1688.

Sibson, R. H., 1977, Fault rocks and fault mechanisms: Journal of the Geological Society of London, v. 133, p. 191-213.

Simpson, C., Law, R. D., Gromet, L. P., Miro, R., and Northrup, C. J., 2003, Paleozoic deformation in the Sierras de Córdoba and Sierra de Las Minas, eastern Sierras Pampeanas, Argentina: Journal of South American Earth Sciences, v. 15, p. 749-764.

Sims, J. P., Ireland, T. R., Camacho, A., Lyons, P., Pieters, P. E., Skirrow, R. G., Stuart-Smith, P. G., Miró, R., 1998. U-Pb, Th-Pb and Ar-Ar geochronology from the southern Sierras Pampeanas, Argentina: implications for the Palaeozoic tectonic evolution of the western Gondwana margin. in The Proto-Andean Margin of Gondwana, Pankhurst, R. J., Rapela, C. W. (Eds.). Geological Society of London, Special Publication 142, p. 259-281.

Thompson, L.M., Spray, J.G., and Kelley, S.P., 1998, Laser probe $^{40}Ar/^{39}Ar$ dating of pseudotachylyte from the Sudbury Structure; evidence for postimpact thermal overprinting in the North Range: Meteoritics and Planetary Science, v. 33, p. 1259-1269

Turner, G., and Cadogan, P. H., 1974, Possible effects of ^{39}Ar recoil in ^{40}Ar-^{39}Ar dating: Procedures of the Fifth Lunar Scientific Conference, v. 2, p. 1601-1615.

Villa, I., 1997, Direct determination of ^{39}Ar recoil distance: Geochimica et Cosmica Acta, v. 61, p. 689-691.

Whitmeyer, S. J., and Simpson, C., 2003, High strain-rate deformation fabrics characterize a kilometers-thick Paleozoic fault zone in the Eastern Sierras Pampeanas, central Argentina: Journal of Structural Geology, v. 25, p. 909-922.

Whitmeyer, S.J., and Simpson, C., 2004, Regional deformation of the Sierra de San Luis, Argentina: Implications for the Paleozoic development of Western Gondwana: Tectonics, 23, TC1005, doi: 10.1029/2003TC001542.

Error: no bibliography entry: d0e2443 found in http://docbook.sourceforge.net/release/bibliography/bibliography.xml